Title	An excitation emission fluorescence lifetime spectrometer using a frequency doubled supercontinuum laser source
Author(s)	Melnikau, Dzmitry; Elcoroaristizabal, Saioa; Ryder, Alan G.
Publication Date	2018-09-03
Publication Information	Melnikau, Dzmitry, Elcoroaristizabal, Saioa, & Ryder, Alan G. (2018). An excitation emission fluorescence lifetime spectrometer using a frequency doubled supercontinuum laser source. Methods and Applications in Fluorescence, 6 (045007). doi: 10.1088/2050-6120/aad9ae
Publisher	IOP Publishing
Link to publisher's version	https://doi.org/10.1088/2050-6120/aad9ae
Item record	http://hdl.handle.net/10379/14649
DOI	http://dx.doi.org/10.1088/2050-6120/aad9ae

An Excitation Emission Fluorescence Lifetime Spectrometer (EEFLS) using a frequency doubled supercontinuum laser source.

Dzmitry Melnikau,[1] Saioa Elcoroaristizabal,[1] and Alan G. Ryder[1*].

[1] Nanoscale Biophotonics Laboratory, School of Chemistry, National University of Ireland – Galway, Ireland.

Running Headline: Fluorescence lifetime spectroscopy with a frequency doubled supercontinuum laser with laser diodes.

* Corresponding author.

Prof. Alan G. Ryder, Nanoscale Biophotonics Laboratory, School of Chemistry, National University of Ireland – Galway, Galway, H91 CF50, Ireland.

Tel: 353-91-492943

Fax: 353-91-552756

Email: alan.ryder@nuigalway.ie

Abstract:

The accurate fluorescence analysis of complex, multi-fluorophore containing proteins requires the use of multi-dimensional measurement techniques. For the measurement of intrinsic fluorescence from tyrosine (Tyr) and tryptophan (Trp) one needs tuneable UV excitation and for steady-state measurements like Excitation Emission Matrix (EEM) simple pulsed Xe lamps are commonly used. Unfortunately, simultaneous multi-dimensional wavelength and time resolved measurement of intrinsic protein fluorescence in the 260 to 400 nm spectral range are challenging and typically required the use of very complex tuneable laser systems or multiple single excitation wavelength sources. Here we have assembled and validated a novel Excitation Emission Fluorescence Lifetime Spectrometer (EEFLS) using a pulsed, frequency doubled, Super-Continuum Laser (SCL) source coupled with a 16 channel multi-anode Time Correlated Single Photon Counting (TCSPC) measurement system. This EEFLS enabled the collection of near complete lifetime and intensity maps over the most important intrinsic protein fluorescence spectral range (λ_{ex} = 260–350 / λ_{em} =300–500 nm). The 4-dimensional ($\lambda_{ex}/\lambda_{em}/I_{(t)}/\tau$) Excitation Emission Fluorescence Lifetime Matrix (EEFLM) data produced can be used to better characterize the complex intrinsic emission from proteins. The system was capable of measuring fluorescence emission data with high spectral (1-2 nm) resolution and had an Instrument Response Function (IRF) of ~650 ps for accurate measurement of nanosecond lifetimes. UV power output was stable after a warm up period, with variations of <2% over 9 hours and reproducible (relative standard deviation RSD <1.5%). This enabled the collection of accurate EEFLM data at low resolution (~12 nm in excitation and emission) in 1-2 hours or high resolution (4 nm) in ~17 hours. EEFLS performance in the UV was compared with a conventional commercial TCSPC system using pulsed LED excitation and validated using solutions of p-terphenyl and tryptophan.

Introduction

Fluorescence spectroscopy is an important measurement tool in the life sciences due to its inherent sensitivity and wide availability of very specific fluorescent probes for a host of different applications [1]. The structural analysis of biological molecules using the emission of intrinsic fluorescence of different natural fluorophores, such as tyrosine (Tyr) and tryptophan (Trp) requires the use of several multi-dimensional measurement techniques. The most widely used steady-state, multi-dimensional measurement techniques are Excitation Emission Matrix (EEM) and Total Synchronous Fluorescence Scan (TSFS) [2] spectroscopy which are widely used for the qualitative and quantitative analysis of complex biogenic liquids such a cell culture media [3-7]. However accurate structural analysis of proteins using intrinsic fluorescence is complicated by spectral overlap. To try and solve this spectral overlap issue we developed Anisotropy Resolved Multi-Dimensional Emission Spectroscopy (ARMES) [8-10] for the analysis of proteins in both simple (e.g. buffer) and complex (in mixtures of small fluorophores) environments. ARMES attempts to solve the overlap problem by the use of anisotropy combined with chemometric analysis, to better resolve emission from different fluorophores, providing information about the environment of each fluorophore.

However, since anisotropy and fluorescence lifetime are intrinsically linked, we need also to measure the complex fluorescence lifetime behaviour of intrinsic protein fluorescence to understand what causes anisotropy changes. In particular, lifetime data can provide information about fluorophore environment and Förster resonance energy transfer (FRET) effects which are very significant in proteins. However, until recently, time-resolved measurements for the analysis of intrinsic protein fluorescence were quite challenging due to the lack of simple and inexpensive pulsed light sources in the 250–300 nm UV region [1]. For intrinsic protein fluorescence measurements, one needs to use excitation sources in the 260–350 nm range, and in the steady-state domain, Xe lamps are probably the most widely available and inexpensive source used. However, lifetime measurements in the time-domain (and particularly for photon counting) require stable picosecond to nanosecond pulsed light sources [11]. Some UV Light Emitting Diode (LED) sources (from 248 to 360 nm) are available, but since these are not tuneable this makes them impractical for EEM type measurements [12]. In the visible and infrared range, tuneable, high brightness sources are typically based on the optical parametric oscillator (OPO) and while OPOs achieve excellent performance they require large pump lasers and can be rather complex and costly to operate and maintain [13]. More recently, robust and relatively low cost

broad bandwidth supercontinuum lasers (SCL) have become available offering a potential solution [13, 14].

The use of a SCL for EEM has been demonstrated [15], however this early system was only operated with visible wavelength excitation. Owen *et al*. [16], demonstrated the use of a UV extended SCL for FLIM, however, this source only generated light at wavelengths >350 nm and thus was incapable of exciting Trp or Tyr. More recently in 2014, frequency doubling of SCL visible output to generate a tuneable UV output between 250 and 430 nm source was demonstrated for microscopy [17]. In this example, a 78 MHz-picosecond pulsed white-light laser was used and output powers in the 1–70 µW range were generated.

Here we demonstrate an Excitation Emission Fluorescence Lifetime Spectrometer (EEFLS) using the tuneable, frequency doubled output (260-350 nm) of a high power SCL and a Time Correlated Single Photon Counting (TCSPC) based measurement system utilizing a multi-anode photomultiplier tube detector. This EEFLS was configured for intrinsic protein fluorescence (Tyr and Trp excitation) measurements and to deliver, rapid and comprehensive emission intensity and lifetime measurements.

Materials & Methods

Materials: P-terphenyl, L-tryptophan, phosphate buffered saline (PBS) tablets, ethanol, Ludox (40 wt. % solution), and high purity water (HPW) were all purchased from Sigma-Aldrich and used without further purification. L-tryptophan stock solutions were prepared using PBS buffer, pH 7.4, and then diluted to a final concentration of 4.5×10^{-5} M. P-terphenyl in ethanol was prepared with a concentration of 7.4×10^{-6} M. All optical measurements were made in 1×0.4 cm pathlength quartz cuvettes (Lightpath Optical, UK) at room temperature, on solutions diluted sufficiently to ensure an absorbance lower than 0.1 in the 1 cm path length to minimize inner filter effects.

Instrumentation (general): Cary 60 UV-Vis and Cary Eclipse Fluorescence spectrophotometers (Agilent Technologies) were used to measure the absorption and fluorescence spectra, respectively. Both were fitted with temperature regulated cuvette holders and measurements were made at 20° ± 0.05 °C. Lifetime data were measured by the new EEFLS and a commercial fluorescence lifetime spectrometer, FluoTime 200 (PicoQuant, Berlin), fitted with a photon counting photomultiplier tube detector (red sensitive, 300-820 nm) and fitted with a pulsed (10 MHz) PLS-295 LED excitation source with ~0.75 µW output power. Fluorescence decay curves from the FluoTime 200 were measured at the magic angle and collected over a 320-400 nm spectral range.

Software and data analysis: One issue with the use of a multi-anode detector was that each detector channel had a different instrument response function (IRF) which complicated the use of re-convolution analysis, making data fitting for the large numbers of decay curves a time-consuming task, and impractical for most routine work. Therefore, for analysis of EEFLS lifetime decays a multi-exponential tail fitting approach was automatically implemented for all the decay curves using an in-house written program working under Matlab v.9.1.0 environment (The Mathworks Inc., Natick, MA). Lifetime data were also fitted by re-convolution and tail fitting using the Fluofit software package (ver. 4.5.3.0, PicoQuant) and compared to results obtained from tail fitting analysis performed using the in-house written MATLAB program. Weighted residuals and χ^2 values were used to judge the goodness of the fitting models. A fit with χ^2 value of less than 1.2 and a evenly distributed residual pattern was considered to be good [1].

EEFLS description: The EEFLS (Figure 1) consisted of a high-power supercontinuum laser (SCL) coupled into a UV wavelength generation unit (SMHP-60.4 and BOX-UVgen2, both from Leukos, France). The SCL produced >4 W of optical power (410–2200 nm) at the fibre output of which ~>700 mW was in the visible region. The nominal repetition rate was 60 MHz and the minimum pulse width was ~ 5 ps. A pulse picker in the SCL gave software selectable pulse rates of 60, 30, 20, 15, 12, and 10 MHz. The SCL was coupled to a frequency doubling unity (BOX-UVgen2, Leukos) that was equipped with an internal flip-flop mirror mount which allowed visible light output (390–750 nm) to be either directed into the frequency doubling crystal or as an external free space beam. The linearly polarized free space UV output (260–350 nm) was then focused into a temperature-controlled cuvette holder (TLC-50F, Quantum Northwest, USA). This cuvette holder was fitted with broad-band anti-reflecting coated fused-silica collimating lens (Balboa Scientific) and then coupled into the PML-SPEC spectrograph/detector through a FC fibre optic connector with a multimode fibre (NA = 0.12, 125 μm diameter), which should depolarize the sample emission [18]. The PML-SPEC spectrograph/detector was fitted with a 600 line/mm grating (blazed at 370 nm) optimized for the 300–650 nm region and controlled by a DCC100 card (all from Becker & Hickl, Berlin, Germany). The detector was a 16 channel multi-anode photomultiplier with a bi-alkali photocathode (optimized for 300–600 nm).
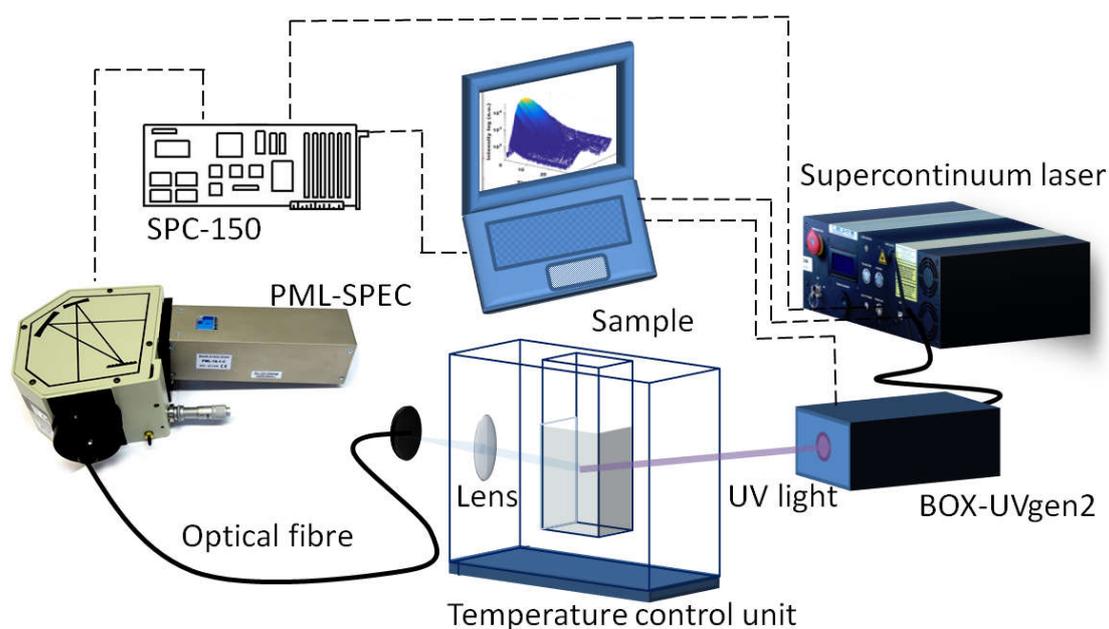
Figure 1: Electronic and optical schematic layout of the EEFLS showing the major components.

A positive voltage output trigger signal from the SCL driver was converted to a negative voltage (–50 mV to –1V) using a PLD-800 TimeHarp sync adapter (PicoQuant). This signal was then attenuated using a 50 Ohm fixed attenuator 50F-006 6dB before being connected to a nanosecond delay unit (Model 7800-7, FastComTec, Germany). The output from the delay unit was then connected to the TCSPC board (SPC-150, Becker and Hickl). The output UV light power (1–14 µW) was measured using a THORLABS PM100 Power meter equipped with S120VC sensor. The UV output was tuneable from 260 to 350 nm with a wavelength accuracy of ± 0.7 nm with band widths varying from 1 to 12 nm which was sufficient for lifetime measurements of molecules in solution. For the UV wavelengths, the full width at half maximum (fwhm) was approximately 650 ps (Figure 2a) as measured using the PML-SPEC (which has a time resolution of ~200 ps). This pulse width was narrow enough for nanosecond lifetime measurements of good accuracy. The UV output power stability (Figure 2b) was measured over three days with 10 hours of continuous operation each day. During the first hour of the laser operation we measured a small decrease in laser power (<5% of the initial value) as the system warmed up. However, over the next nine hours the laser power stabilized, and the variation was ~2% which was sufficient for the long data collection times required for high resolution lifetime maps to be collected. Over the three days of testing a relative standard deviation of <1.5% was obtained for the UV power output demonstrating good reproducibility and stability.

A time and wavelength resolved matrix (Figure 2c/d) of a scattering solution (Ludox, 1% w/w) for an excitation wavelength of 330 nm measured using the EEFLS gave a visual representation of the time and spectral characteristics of the laser and detection system.
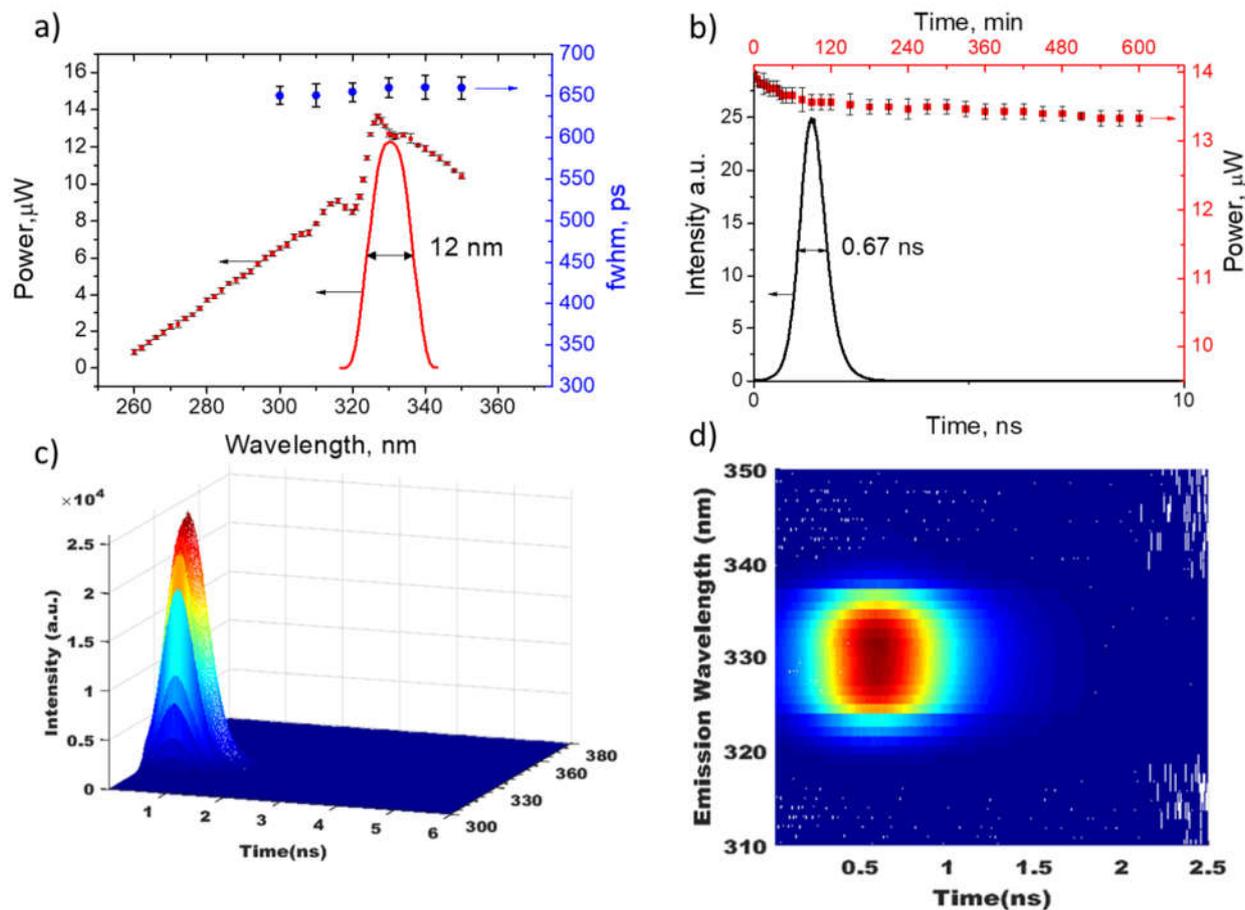

Figure 2: *a).* Power (measured at the cuvette holder) versus wavelength for the UV output (red squares). Dependence of the full width at half maximum of instrument response function (IRF) on wavelength (blue circles). Spectra of supercontinuum laser at 330 nm (red curve) measured using the EEFLS. *b).* Output pulse profile of the laser at 330 nm (black curve); SCL power stability at 330 nm over 10 hours (red squares). c) and d) Simultaneous time and wavelength resolved surface plot of the frequency doubled SCL output at 330 nm measured using a scattering solution (Ludox 1% w/w).

The EEFLS was configured during data acquisition to obtain excitation emission fluorescence lifetime matrix (EEFLM) spectra with a resolution of 1 and 2 nm along the excitation and emission axes respectively. The excitation wavelength change was implemented in the SCL control software. The multi-anode detector (16 channels) had a spectral range of ~200 nm with a resolution of ~11-13 nm.   To improve emission spectral resolution, the grating angle was manually changed in small increments [one division of the grating rotation scale corresponded to a shift of 2 nm], and the 16-channel data re-collected to generate sufficient data to produce

fluorescence spectra with a spectral resolution of 2 or 4 nm. For 4 nm resolution spectra with ~20K max counts of Trp over the 300-500 nm range we collected 3 sets of spectra, each taking ~ 30 minutes at each excitation wavelength. The 16×3 decay curves were interleaved to produce the final emission spectrum for each excitation wavelength. For example, in the case of Trp, using 11 excitation wavelengths (260 to 300 nm) it took around 17 hours to complete an EEFLM measurement. For higher resolutions there was a significant increase in collection times e.g. for a 2 nm resolution EEFLM we needed to collect six sets of emission spectra (16×6-point) and double the number of excitation wavelengths, leading to a four-fold increase in measurement time (~68 hours). However, these long acquisition times were only required for the collection of high count number/low noise data for high accuracy multi-exponential lifetime fitting that would not be necessary for all experiments. For screening type experiments (fixed ~12 nm resolution in emission, i.e. no grating changes) or for those comparing relative changes, then lower count numbers would be acceptable (similar to lifetime imaging type experiments) and in this case 5K counts in the channel of maximum intensity might suffice, reducing the acquisition times even further to 1-2 hours depending on the sample.

EEFLM Data structure: Data were collected as a series of lifetime decay curves over a range of emission wavelengths (λ_{em}= 292 – 500 nm, $\Delta\lambda$= 4 nm) generating a two-way array of size 48 × 4096 (λ_{em} × time data points). The combination of eleven emission lifetime matrices collected at different excitation wavelengths (λ_{ex} = 260 – 300 nm, $\Delta\lambda$= 4 nm) generated a three-way, EEFLM array, of size 11 × 48 × 4096 for each sample (Figure 3a). Since the EEFLM were measured with a multi-channel detector with different time shifts (see SI, Figure S1) and background intensity offsets (see SI, Figure S2) for each detection channel, some data pre-processing was required prior to data analysis (Figure 3b-d). To correct for the small time shifts 0.01-0.2 ns (see SI) between the detector channels we used a correlation optimized shifting *(coshift)* algorithm [19].   For background correction, the background was measured for each detection channel in the EEFLM at a point where the emission had decayed completely and then subtracted from the measured lifetime decays. For example, for the Trp and p-terphenyl fluorophores the background region selected was between 25–30 ns for a 30 MHz repetition rate. Figure S2 in the SI shows the dark background acquired during a 30-minute measured (a similar time used in most of our experiments) and this indicated that background signal was independent of the time domain but varied according to the different detection channels.

The PML_SPEC detector system covered a 200 nm spectral range, as a result of which we have a relatively large number of data points at the boundaries of the fluorescence emission, where the fluorescence intensity was very low, and it was not possible to obtain reliable lifetime data.

Therefore, lifetime decay curves with maximum intensity of less than 5% of the most intense emission decay curve in the EEFLM were removed before implementing the fitting routine (Figure 3b). For the high-resolution datasets where the maximum intensity of the decay curve intensity was 20K, all points in the EEFLM which had a decay intensity of <1K counts were excluded from fitting.
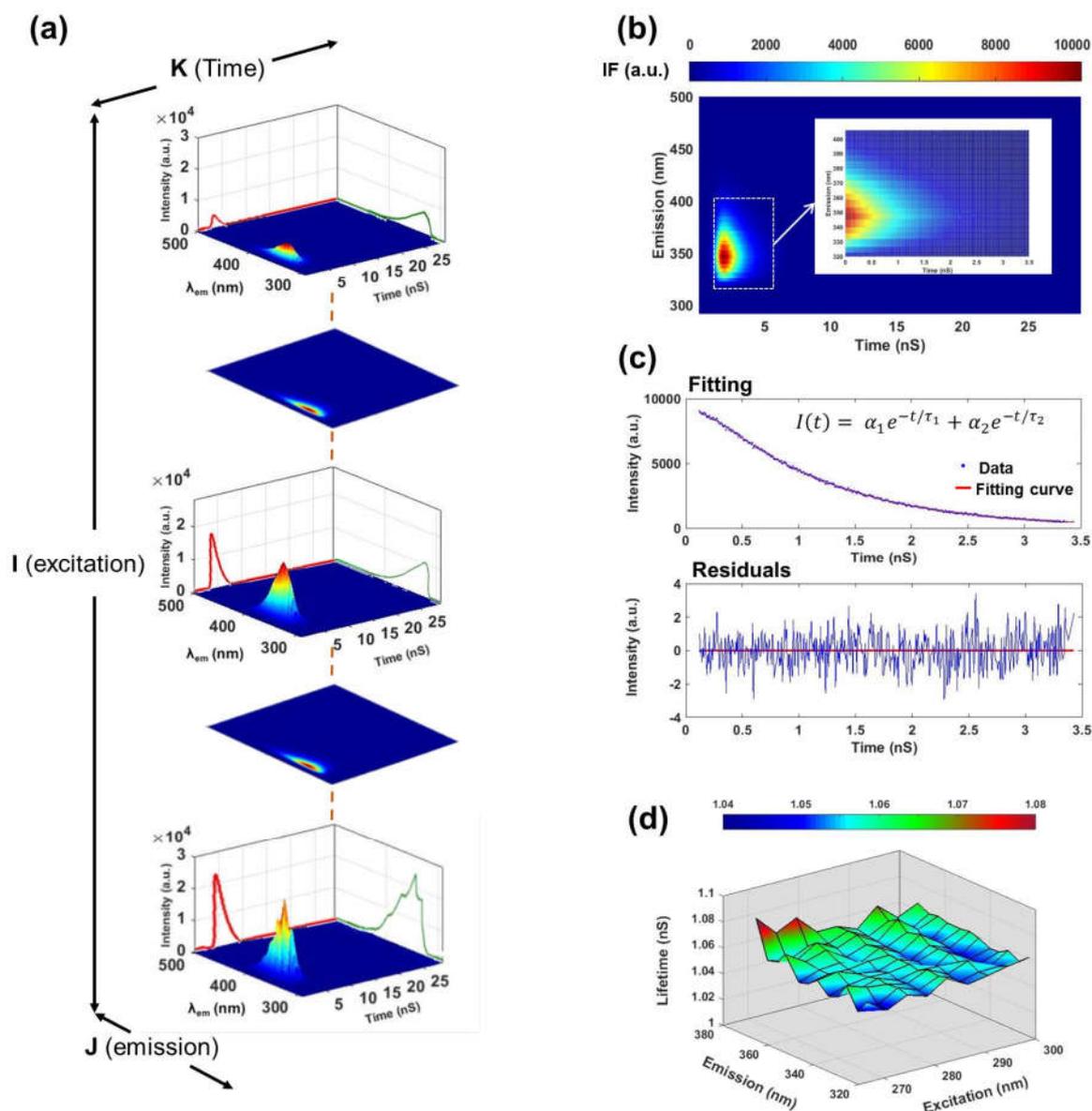

Figure 3: *a).* Representation of the EEFLM data, which consists of fluorescence intensity as a function of excitation and emission wavelengths and time decay curves measured by the EEFLS;   Scheme of data treatment and analysis: *b).* Pre-processed Lifetime Emission Matrix at a single excitation wavelength, with the expanded region showing the data selected for fitting;   *c).* Tail fit using in-house written MATLAB code of lifetime decay curve;   *d).* EEFLM map for p-terphenyl.

Lifetime emission decay data analysis of intrinsic protein fluorescence generally involves the use of multi-exponential decay models [20, 21] because of multiple fluorophores and the heterogeneity of the fluorophore environment.   Here, the lifetime decays at each emission wavelength (Figure 3b) were fitted to a single or bi-exponential function using the MATLAB curve fitting toolbox using a non-linear least squares method based on Trust-Region algorithm [22]. The MATLAB in-house program was designed to pre-process and automatically fit the large numbers of decay curves obtained from this EEFLS. The fit models were used to calculate the corresponding amplitude and lifetime at each emission wavelength for the range of excitation wavelengths as follows:

$$I(t) = \sum_{i=1}^{n} \alpha_i e^{-t/\tau_i} \qquad (1)$$

where $I(t)$- intensity decay curve, α_i-the amplitude corresponding to lifetime τ_i

In the case of bi-exponential fitting, two different average lifetimes were calculated: the intensity weighted average lifetime $\langle\tau\rangle_f$ (Eq.2) and the amplitude weighted average lifetime, $\langle\tau\rangle_a$ (Eq. 3). $\langle\tau\rangle_f$ is, which equals the average amount of time for which the fluorophores remain in their excited state after the onset of excitation whereas $\langle\tau\rangle_a$ is proportional to the steady state intensity [23]. This is applicable when the FRET efficiency is being calculated based on the lifetimes of the donor in the presence and absence of the acceptor molecule [23]:

$$\langle\tau\rangle_f = \frac{\sum_{i=1}^{n} \alpha_i \tau_i^2}{\sum_{i=1}^{n} \alpha_i \tau_i} = \frac{\alpha_1 \tau_1^2 + \alpha_2 \tau_2^2}{\alpha_1 \tau_1 + \alpha_2 \tau_2} \qquad (2)$$

$$\langle\tau\rangle_a = \frac{\sum_{i=1}^{n} \alpha_i \tau_i}{\sum_{i=1}^{n} \alpha_i} = \frac{\alpha_1 \tau_1 + \alpha_2 \tau_2}{\alpha_1 + \alpha_2} \qquad (3)$$

Once the lifetime (or average lifetime) at each excitation and emission wavelength had been calculated an EEFLM map Figure 3d could be plotted. Using this tail fit procedure, we can reliably measure fluorescence lifetimes comparable to the fwhm of the system IRF which was approximately 650 ps in the UV. When more accurate fitting than this is required, IRF data can be acquired and reconvolution fit analysis employed. This should enable the accurate measurement of lifetimes down to approximately 100 ps [11].

Steady-state EEM plots: One can also extract from the EEFLM data the corresponding steady-state excitation and emission matrix (EEM) fluorescence spectra. Since the UV output power was wavelength dependent, to obtain an EEM we normalized the intensity of each fluorescence

emission spectrum according to the excitation laser power for each excitation wavelength. This data can then be used to compare measurements against conventional steady-state spectrometers (see SI Figure S3). However, this spectrometer and the conventional fluorescence spectrometers need to be standardised first, to account for instrumental effects before this can be achieved. This process is underway using a series of certified reference standards [24], however, the process is complicate by the wide spectral ranges involved in the EEFLM data.

Results and Discussion

1. EEFLS performance

Integration of the SCL-UV box with the PML-SPEC and SPC-150 was reasonably straightforward and the optical components were generally off the shelf components which were easily aligned. We used a fibre coupled optical path on the emission as this facilitated easy assembly and alignment, however, it does reduce light throughput leading to longer data collection times. We did not use any excitation or emission filters in the EEFLS and we did not find much evidence so far for issues with excitation light scatter contamination or parasitic emission from the UV source. This can be attributed to the use of fibres in the emission path and the spectrograph provided sufficiently good stray light rejection.

The power stability data (Figure 2b) indicated that the system needed about one hour to stabilise, after which it then remained relatively stable for a long time (> 9 hours) enabling high quality EEFLM data to be collected. We used two different SCL laser sources (both from Leukos) during the course of this work, which produced different UV output powers from the same UV-BOX. These were a fixed frequency (30 MHz) 4W Leukos SCL with a visible output spectral range of 500–2400 nm and a variable frequency (with pulse picker) 4W Leukos SCL with a visible output of spectral range 410–2400 nm. The microwatt UV output powers while low in the 260–290 nm region (0.8 to 5 µW) were sufficient for most solution samples used here and for typical micromolar amino acid or protein samples. Increasing the SCL output power would reduce measurement time, however, this would also cause increased photobleaching. A more correct solution will be to increase the light collection efficiency on the emission side via the use of high numerical aperture collection optics and modification of the PML-SPEC input optics. However, a comparative photobleaching study using Trp in PBS buffer (see Figure S-5, SI) indicated that the degree of photobleaching during EEFLM measurements was less than that experienced with a standard fluorimeter (Cary Eclipse, Agilent). Even after 8 hours illumination (8.25 µW, 60 MHz pulse rate, at the excitation maximum) the emission intensity had only dropped by ~3.5%. It is known that Trp in buffer solution (at pH 7.8) has a reasonably high

photobleaching quantum efficiency of approximately 6.5% [25].   However, Trp photostability increases significantly in proteins, which suggests that photobleaching should be acceptable in protein studies using the EEFLS even over relatively long acquisition times.

This current EEFLS configuration is however, a collection of manually operated subsystems which change of the SCL excitation wavelength (in the software) and changing of PML-SPEC grating angle to provide high spectral resolution. This means that the operator needs to be physically present during the long measurement times.

2.   EEFLS Validation.

The EEFLS was designed and configured for studying the intrinsic fluorescence of proteins in the UV and therefore system performance in the lifetime domain had to be validated using both a simple lifetime standard, p-terphenyl, which had a mono-exponential lifetime decay and the more complex emission from the key amino acid, tryptophan (Trp). The photo-physical properties of p-terphenyl and Trp are well described in the literature [20, 26-31] and Figure 4 shows the absorption and fluorescence spectra of p-terphenyl in ethanol and Trp in buffer. P-terphenyl was selected as the lifetime standard as its emission spectrum overlapped very well with the emission spectrum of Trp, the dominant fluorophore producing intrinsic fluorescence in most proteins. A second reason for its use was that p-terphenyl in PMMA was available as a solid reference standard from various vendors and thus can be used as a solid lifetime and anisotropy standard (e.g. Agilent part number: 6610010300). This was important as it enabled polarization effects (due to the linearly polarized UV excitation light in the EEFLS) to be rapidly identified.
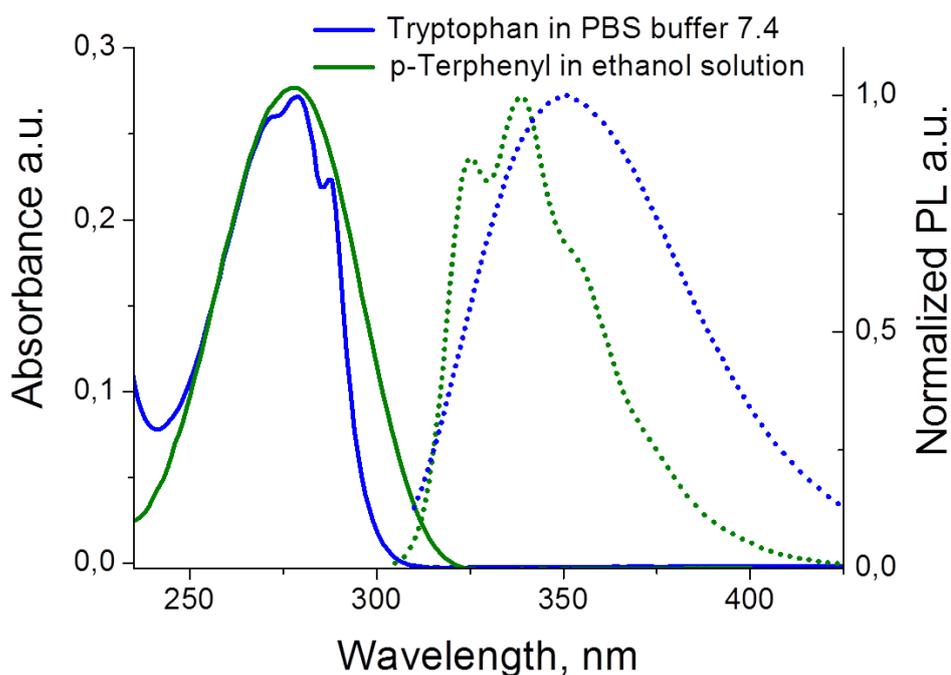
Figure 4:   Absorption (solid lines) and fluorescence emission (dotted lines) spectra of p-terphenyl in ethanol solution (green) and Trp (blue) in PBS buffer pH=7.4.

The p-terphenyl solution lifetime data (λ_{ex} = 295 nm) obtained using the EEFLS were compared with the data of the same sample measured using the FluoTime 200 with LED excitation (Figure 5a/b). The decay curves were tail fitted for the EEFLM and reconvolution fitted for the FluoTime 200 data as described above, and then compared (Figure 5a/b and Table 1). The p-terphenyl lifetime values at the fluorescence maximum obtained using both systems at 295nm excitation was 1.055 ± 0.004 ns and in good agreement with the literature [26, 27]. A comparison (Table 1) between the lifetimes for different emission wavelengths (320 to 370 nm, 10 nm step) also showed excellent agreement (< 1% difference) and all data were well fitted (χ^2 <1.2). To compare the similarity in the performance among the methods, a comparison of the lifetime values as measured by each system was tested using a paired *t*-test [32], which indicated that there were no significant differences (p>0.05). This excellent agreement confirmed that all the optical and electronic components of the EEFLS were well-aligned, and that accurate lifetime data was being produced.   These measurements also validated the use of the MATLAB based tail-fitting algorithm and pre-processing procedures.
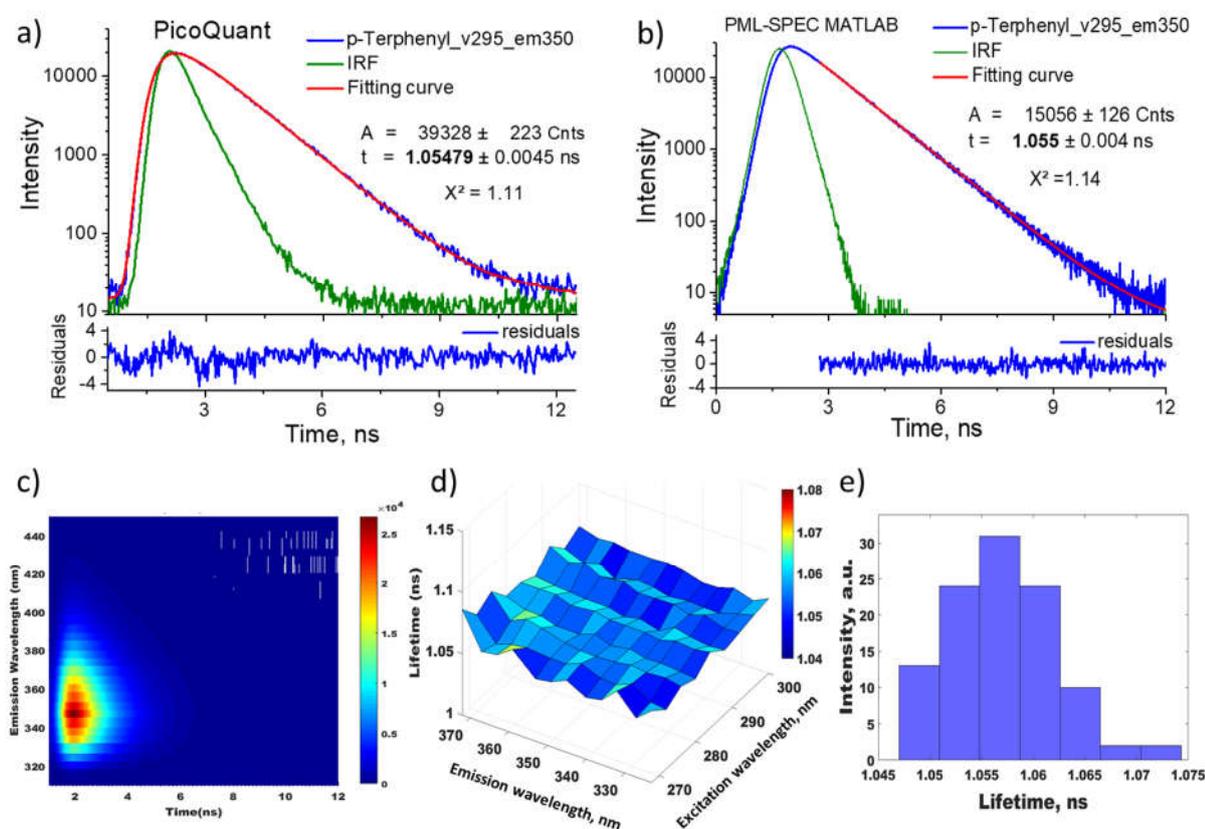
Figure 5: Lifetime decay curves (blue), IRF traces (green), and fit curves (red) of p-terphenyl in ethanol excited at 295 nm, obtained using: ***a).*** FluoTime 200, TCSPC system with a PLS-295 LED excitation source; fitted by re-convolution; ***b).*** EEFLM data fitted using in-house MATLAB program; ***c).*** Time, emission wavelength, intensity map of p-terphenyl fluorescence (λ_{ex}=295 nm) measured using the EEFLS; ***d).*** Fluorescence lifetime map of p-terphenyl in ethanol obtained using EEFLS; ***e).*** Fluorescence lifetime histogram obtained from single exponential fitting of p-terphenyl in ethanol decay curves at each point in the excitation emission matrix. The bar heights represent the relative statistical weights.

Table 1: Mono-exponential lifetimes for p-terphenyl in ethanol (7.4×10^{-6} M) with λ_{ex}=295 nm, measured using the FluoTime 200 and EEFLS for different emission wavelengths.

Wavelength	IRF reconvolution fit (PQ)		Tail fit (EEFLM)	
	τ_1 *(ns)*	χ^2	τ_1 *(ns)*	χ^2
320	1.056 ± 0.004	1.12	1.054 ± 0.003	1.12
330	1.056 ± 0.004	1.06	1.052 ± 0.002	0.98
340	1.057 ± 0.005	1.13	1.051 ± 0.003	1.13
350	1.055 ± 0.004	1.11	1.055 ± 0.004	1.14
360	1.055 ± 0.004	1.08	1.058 ± 0.002	0.97
370	1.056 ± 0.005	1.16	1.058 ± 0.002	0.96

At each excitation wavelength, the EEFLS generated a time versus emission wavelength map (Figure 5c), which once repeated for a range of excitation wavelengths and fitted with an appropriate lifetime model produced an EEFLM map (Figure 5d). This p-terphenyl EEFLM data showed that in ethanol there was a constant mono-exponential lifetime over the excitation (270-300 nm) and emission range (320-370) sampled [26, 27]. This is illustrated by the fluorescence lifetime histogram, which showed a very narrow lifetime distribution of 1.057 ± 0.005 ns (Figure 5e). This narrow lifetime distribution for the different excitation and emission wavelengths indicated a good and stable performance of the EEFLS over the important spectral range where the intrinsic fluorescence of amino acids occurs. P-terphenyl in PMMA (solid sample) lifetime (λ_{ex}=295 nm) measured by the FluoTime 200 and EEFLS for different emission wavelengths was also evaluated (Table S1, SI). Here the data were reasonably well fitted (χ^2 <1.2 apart from one fit, for which the decay intensity was relatively low, ~2K) and showed small differences (< 4%) for the lifetime values which was statistically insignificant (p>0.001). This indicated that the

polarization effects were small, presumably due to the scrambling effect of the multi-mode fibre used in the emission arm of the EEFLS.

3.   EEFLM measurements on Tryptophan.

While the mono-exponentially decaying p-terphenyl validated general system performance and the tail fitting MATLAB algorithm, it was not entirely suitable for fully validating the system for protein studies where complex emission decays are the normally present. In this regard, it was important to note that intrinsic fluorescence of proteins mainly caused by Trp, which has a complex emission and displays at least bi-exponential behaviour in buffer solution. Therefore, to ensure that the proposed procedure was robust and that EEFLS was sufficiently sensitive to identify subtle changes in emission properties we used Trp as the second standard for instrument validation. The recovered bi-exponential fit Trp lifetimes ($\lambda_{ex}/\lambda_{em}$ = 295/350 nm) using the FluoTime 200 and EEFLS systems were τ_1= 0.94 ns, τ_2= 3.09 ns and τ_1= 0.88 ns, τ_2= 3.08, respectively (Figure 7a/b). The bi-exponential decay model provided a good fit with reasonable chi-squared values suitable for system comparison. The Trp bi-exponential decay with lifetimes of τ_1= 0.5 – 0.8 ns and τ_2= 3.1 – 3.5 ns [20, 28, 29, 33] can be ascribed to the presence of different rotamer populations [20, 29, 30, 33]. Figure 6 shows the comparison of the Trp lifetimes and corresponding amplitudes versus emission wavelengths measured by the EEFLS and FluoTime 200 with the different fitting methods.
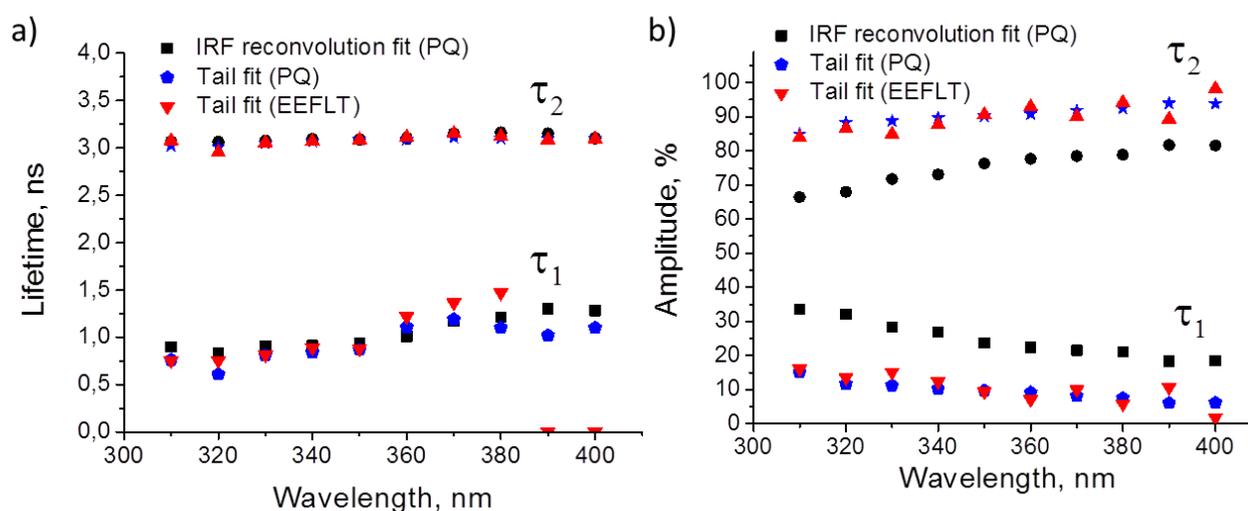

Figure 6: Emission wavelength (λ_{ex}=295 nm) dependence of Trp: *a).* lifetimes τ_1 and τ_2, and *b).* corresponding amplitudes, from EEFLS data fitted using MATLAB and by FluoTime 200 (PQ) data fitted by IRF re-convolution and tail fitting using the Fluofit software. A double exponential model was used in all cases.

It was observed that the lifetime results produced by both systems and different fitting methods/software were very similar (Figure 6). This was particularly noticeable for the longer τ_2 lifetime (<3% difference) which was not statistically significant (p>0.05). There were some differences, however, in the short lifetime (τ_1) measured using the EEFLS at longer wavelengths (390-400 nm), which was a fitting artefact caused by relatively low emission intensities at these wavelengths. A more accurate result was obtained using the FluoTime 200 system with IRF reconvolution fitting, even though χ^2 values in this case were significantly higher (1.28 – 1.51) as we fitted the full decay curve as opposed a shorter tail fit (see SI, Table S2). Nevertheless, the recovered Trp lifetime components were very similar for the two systems and to values reported in the literature [20, 28, 29, 33].

One does however, have to be careful with the interpretation of the tail fit components (i.e. amplitudes) as tail fitting is always likely to overestimate the contribution of the longer-lived species (Figure 6b). This also results in longer average lifetimes being calculated (Figure S-6, SI) and therefore care needs to be taken in their use for calculation of accurate FRET efficiencies. Despite this issue, the EEFLM tail fit provides a relatively quick method to assess the general FRET changes across the full emission space of Trp and Tyr (and therefore most proteins). As mentioned previously when more accurate lifetime data is required, IRF data will be acquired and re-convolution fitting applied to extract the true lifetime contributions.
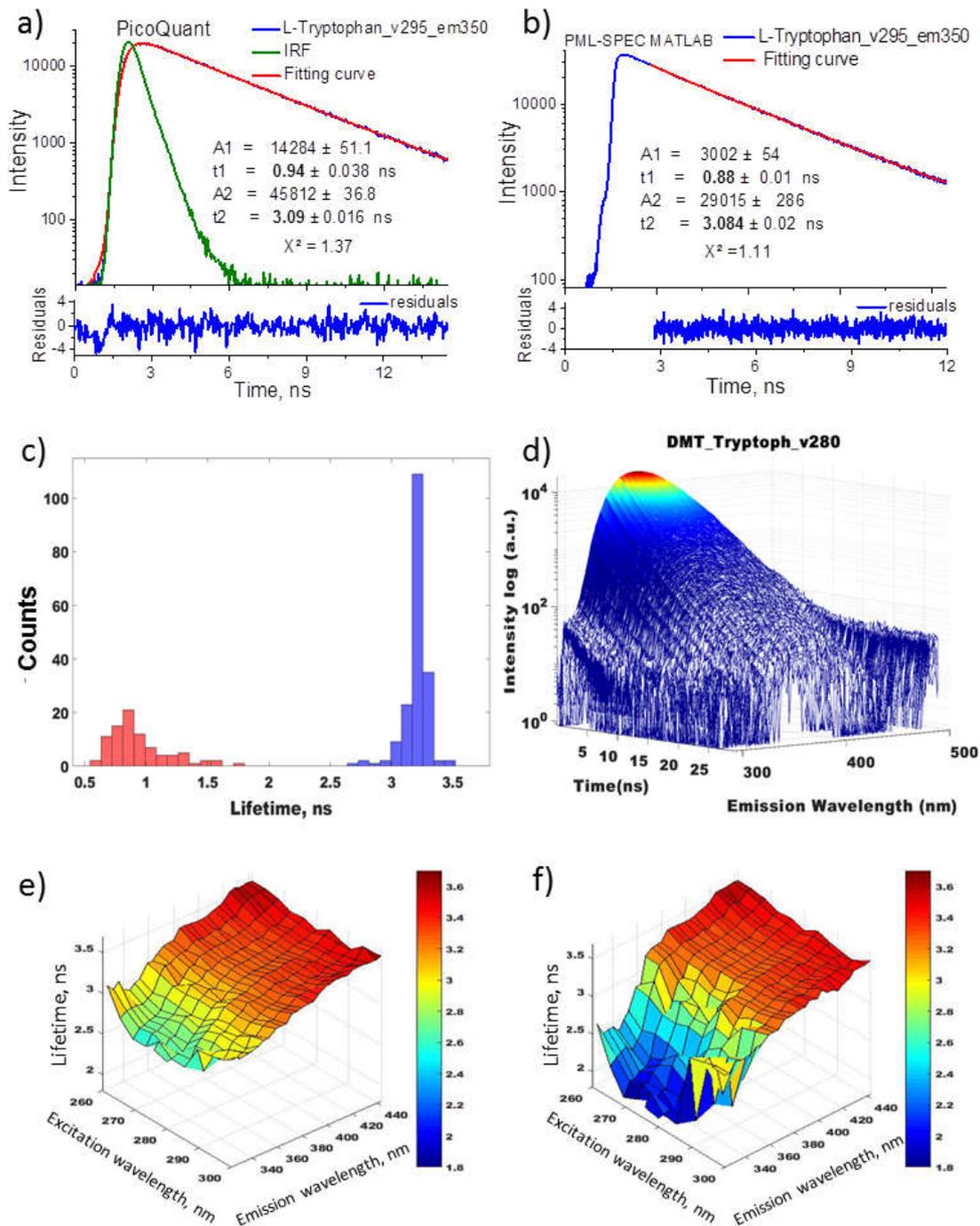
Figure 7: Lifetime decay curve of Trp in PBS buffer solution, pH=7.4, excited at 295 nm (blue curve), obtained using: ***a).*** FluoTime 200/LED excitation; fitted using re-convolution with IRF (green curve) using Fluofit software; and ***b).*** EEFLS system, fitted using in-house MATLAB code; ***c).*** Trp lifetime histogram obtained from a bi-exponential fitting of the decay curves at each point in the EEM. The bar heights represent the relative statistical weights of the two lifetime components; ***d).*** Time, emission wavelength, intensity matrix of Trp fluorescence (λ_{ex}=280 nm) measured using the EEFLS; EEFLM plots of Trp for: ***e)***. Intensity averaged lifetime, $\langle\tau\rangle_f$ and ***f).*** Amplitude averaged lifetime, $\langle\tau\rangle_a$.

Variations in the two components of the Trp lifetime decay was determined by the effectiveness of quenching processes for the different rotamers. Trp emission in neutral solutions can be quenched by an intramolecular process involving the indole ring and the positively charged ammonium group [29, 30, 33, 34]. In some studies, [29, 30, 34, 35] a significant increase in Trp lifetime at high pH (pH=8 – 10) was shown to be caused by a reduction in Trp self-quenching by the ammonium group. This resulted from progressive dissociation of the ammonium group to the neutral form with increasing pH. Similarly a lifetime study of Trp complexed with 18-Crown-6, (which prevents quenching by the ammonium group) showed, that this complex had a mono-exponential decay [36]. Self-quenching processes for the different Trp rotamers suggested that for Trp is more likely to display a distribution of lifetimes rather than discrete lifetime values across the emission space and this was confirmed by the Trp lifetime histogram (Figure 7c) recovered from the EEFLM. The shorter lifetime component (τ_1) with a maximum of 0.9 ns is much broader compared to the lifetime distribution of the longer component (τ_2) with a maximum of 3.2 ns. This was probably due to the fact that amplitude of τ_2 was much greater than that of τ_1, which resulted in a more precise lifetime value. More detailed investigations of Trp emission are underway which will provide a deeper insight into this rotamer issue and the consequences for protein fluorescence.

Using the EEFLS we can accurately, simultaneously measure wavelength and lifetime resolved spectra of Trp which covered most of the spectral region where intrinsic protein fluorescence occurs. Overlaying EEM and $\langle \tau \rangle_a$ lifetime map (Figure S4, SI) provides a more complete picture of the emission behaviour of Trp and to help us better understand the photophysical properties of complex emitters like Trp. Trp lifetimes and their amplitudes also depended on the emission and excitation wavelengths (Figure 7e-f). The $\langle \tau \rangle_f$ and $\langle \tau \rangle_a$ lifetime maps (Figure 7e/f) were very different for λ_{em} ~340 nm (320 to 380 nm), which was most likely caused by self-quenching via amino groups [29, 30, 33, 34]. At the longer emission wavelengths (380 to 440 nm) the small increases in both $\langle \tau \rangle_f$ and $\langle \tau \rangle_a$ were probably due to solvent relaxation effects [1]. Along with the emission wavelength lifetime dependence, we also observed a variation in the Trp average lifetimes with the excitation wavelength. A small dip in the 270 – 280 and 350 nm region for excitation and emission respectively was clearly visible. This was especially evident for the $\langle \tau \rangle_a$ data (Figure 7f). It was noteworthy that this dip was observed in the region where a decrease in Trp anisotropy also occurred [37], and this could be associated with energy transfer between the two electronic transitions ^1L_a and ^1L_b states.

Conclusions

This Excitation Emission Fluorescence Lifetime Spectrometer (EEFLS) was a relatively simple, modular setup that allows one to make a fast, complete and accurate analysis of the fluorescence intensity and lifetime data in the UV region, 260-350 and 300-500 nm $\lambda_{ex}/\lambda_{em}$ range where most intrinsic fluorescence of proteins occurs. Using a p-terphenyl lifetime standard and Trp solutions we validated EEFLS performance of and the lifetime data acquired agreed with literature values and with data collected using a commercial TCSPC system. The EEFLS measured lifetime (from tail-fit analysis) of p-terphenyl in ethanol standard was constant over the wide UV excitation/emission range sampled which demonstrated that the system worked effectively in the required spectral ranges. For the more complex Trp case, lifetime values for both components obtained using FluoTime 200 and EEFLS were very similar and in good agreement with the literature [20, 28, 29, 33]. We also demonstrated that the use of tail fitting (using in-house developed MATLAB routines) generated very similar results to that obtained using reconvolution fitting for nanosecond lifetimes. The tail-fitting approach enabled the rapid, accurate fitting of the large numbers of decay curves generated by the system (typically >100 curves) required for spectral analysis. To extract accurate lifetimes and contributions however (particularly for complex proteins intrinsic emission) the slower IRF reconvolution fitting process needs to be used. This combined with a variety of fixed species models and lifetime distribution can be applied [38-40] to investigate different aspects of energy transfer and quenching.

EEFLS measurement times were determined by the spectral and temporal accuracy required by the particular experiment. For fast photophysical screening experiments (10×16 EEFLM) with low emission resolution (~12 nm) it was feasible to collect the data for 10 excitation wavelengths, in 5-6 hours depending on sample intensity. This was sufficient to quickly estimate the temporal and spectral characteristics of the sample over a relatively wide excitation (~100 nm) and emission (~200 nm) range. This then can be then supplemented with slower, high resolution measurements on selected spectral regions to acquire more precise lifetime data. The data array ($\lambda_{ex}\times\lambda_{em}\times I_t\times\tau$) generated by the EEFLS can generate a wide variety of different output maps according to the methods used to fit the decay data. Further detailed studies are underway to use the EEFLS to better understand the contribution of various rotamers and electronic transitions such as ^1L_a and ^1L_b states to the temporal and spectral characteristics of Trp fluorescence.

One rationale for collecting high wavelength resolution EEFLM data is the desire to take a more multi-dimensional approach to complete emission data analysis and leveraging the power of multivariate chemometric techniques such as Multivariate Curve Resolution [41], and Parallel Factor (PARAFAC) [42]. These curve fitting methods require high resolution data for best

performance, and they could provide new routes for better interpreting the complex intrinsic emission generated by proteins. The next stage of the EEFLS hardware development will involve better integration of the various sub-systems to enable a more automated experimental procedure and also the optimisation of light throughput efficiency, possibly via the use of free space optics rather than fibre coupling. This should facilitate faster, more efficient measurements, and reduce the potential for photobleaching.

Acknowledgements

References:

[1] J.R. Lakowicz, Principles of Fluorescence Spectroscopy, 3rd Edition ed., Springer, New York, 2006.
[2] D. Patra, A.K. Mishra, Recent developments in multi-component synchronous fluorescence scan analysis, Trac-Trends in Analytical Chemistry, 21 (2002) 787-798.
[3] P.W. Ryan, B. Li, M. Shanahan, K.J. Leister, A.G. Ryder, Prediction of Cell Culture Media Performance Using Fluorescence Spectroscopy, Anal. Chem., 82 (2010) 1311-1317.
[4] B. Li, P.W. Ryan, M. Shanahan, K.J. Leister, A.G. Ryder, Fluorescence excitation-emission matrix (EEM) spectroscopy for rapid identification and quality evaluation of cell culture media components, Appl. Spectrosc., 65 (2011) 1240-1249.
[5] C. Calvet, B. Li, A.G. Ryder, Rapid quantification of tryptophan and tyrosine in chemically defined cell culture media using fluorescence spectroscopy., J. Pharm. Biomed. Anal., 71 (2012) 89-98.
[6] A. Calvet, B. Li, A.G. Ryder, A rapid fluorescence based method for the quantitative analysis of cell culture media photo-degradation, Anal. Chim. Acta, 807 (2014) 111-119.
[7] A. Calvet, A.G. Ryder, Monitoring cell culture media degradation using surface enhanced Raman scattering (SERS) spectroscopy, Anal. Chim. Acta, 840 (2014) 58-67.
[8] R.C. Groza, A. Calvet, A.G. Ryder, A fluorescence anisotropy method for measuring protein concentration in complex cell culture media, Anal Chim Acta, 821 (2014) 54-61.
[9] Y. Casamayou-Boucau, A.G. Ryder, Extended wavelength anisotropy resolved multidimensional emission spectroscopy (ARMES) measurements: better filters, validation standards, and Rayleigh scatter removal methods, Methods Appl Fluoresc, 5 (2017) 037001.
[10] Y. Casamayou-Boucau, A.G. Ryder, Accurate anisotropy recovery from fluorophore mixtures using Multivariate Curve Resolution (MCR), Anal. Chim. Acta, 1000 (2018) 132-143.

[11] D.V. OConnor, D. Phillips, Time-Correlated Single Photon Counting., Academic1984.

[12] J.J. Huang, H.C. Kuo, S.C. Shen, Nitride semiconductor light-emitting diodes (LEDs) Materials, technologies and applications Preface, Nitride Semiconductor Light-Emitting Diodes (Leds): Materials, Technologies and Applications, (2014) Xxiii-Xxvi.

[13] Supercontinuum Generation in Optical Fibers, Cambridge University Press, Cambridge, UK. , 2010.

[14] R. Fenske, D.U. Nather, R.B. Dennis, S.D. Smith, The Supercontinuum Laser as a Flexible Source for Quasi-Steady State and Time Resolved Fluorescence Studies, in: K. Tankala, J.W. Dawson (Eds.) Fiber Lasers Vii: Technology, Systems, and Applications, Spie-Int Soc Optical Engineering, Bellingham, 2010.

[15] W. Wang, Z. Wu, J. Zhao, H. Lui, H. Zeng, A rapid excitation-emission matrix fluorometer utilizing supercontinuum white light and acousto-optic tunable filters, Rev. Sci. Instrum., 87 (2016).

[16] D.M. Owen, E. Auksorius, H.B. Manning, C.B. Talbot, P.A.A. de Beule, C. Dunsby, M.A.A. Neil, P.M.W. French, Excitation-resolved hyperspectral fluorescence lifetime imaging using a UV-extended supercontinuum source, Opt. Lett., 32 (2007) 3408-3410.

[17] M. Bradler, F.D. Nielsen, C.E. Eckert, E. Riedle, A broad and tunable 250-to 430-nm source for microscopy and lifetime measurements by frequency doubling of a 78-MHz-picosecond white-light laser, Applied Physics B-Lasers and Optics, 116 (2014) 875-882.

[18] D.V. Kizevetter, Waveguide theory of the depolarization of the radiation of multimode fiber lightguides, Journal of Optical Technology, 73 (2006) 820-822.

[19] V.G. van Mispelaar, A.C. Tas, A.K. Smilde, P.J. Schoenmakers, A.C. van Asten, Quantitative analysis of target components by comprehensive two-dimensional gas chromatography, J. Chromatogr. A, 1019 (2003) 15-29.

[20] J.M. Beechem, L. Brand, Time-Resolved Fluorescence Of Proteins, Annu. Rev. Biochem, 54 (1985) 43-71.

[21] A. Brockhinke, R. Plessow, P. Dittrich, K. Kohse-Hoinghaus, Analysis of the local conformation of proteins with two-dimensional fluorescence techniques, Applied Physics B-Lasers and Optics, 71 (2000) 755-763.

[22] R.W.K. Leung, S.C.A. Yeh, Q.Y. Fang, Effects of incomplete decay in fluorescence lifetime estimation, Biomedical Optics Express, 2 (2011) 2517-2531.

[23] A. Sillen, Y. Engelborghs, The correct use of "average" fluorescence parameters, Photochem. Photobiol., 67 (1998) 475-486.

[24] U. Resch-Genger, D. Pfeifer, C. Monte, W. Pilz, A. Hoffmann, M. Spieles, K. Rurack, J. Hollandt, D. Taubert, B. Schonenberger, P. Nording, Traceability in fluorometry: Part II. Spectral fluorescence standards, Journal of Fluorescence, 15 (2005) 315-336.

[25] M. Lippitz, W. Erker, H. Decker, K.E. van Holde, T. Basche, Two-photon excitation microscopy of tryptophan-containing proteins, Proc. Natl. Acad. Sci. U.S.A., 99 (2002) 2772-2777.

[26] J.R. Lakowicz, H. Cherek, Dipolar Relaxation in Proteins on the Nanosecond Timescale Observed by Wavelength-Resolved Phase Fluorometry of Tryptophan Fluorescence, J. Biol. Chem., 255 (1980) 831-834.

[27] J.R. Lakowicz, H. Cherek, Resolution of Heterogeneous Fluorescence from Proteins and Aromatic-Amino-Acids by Phase-Sensitive Detection of Fluorescence, J. Biol. Chem., 256 (1981) 6348-6353.

[28] J.R. Lakowicz, R. Jayaweera, H. Szmacinski, W. Wiczk, Resolution of two emission spectra for tryptophan using frequency-domain phase-modulation spectra, Photochem. Photobiol., 50 (1989) 541-546.

[29] M.R. Eftink, Y.W. Jia, D. Hu, C.A. Ghiron, Fluorescence Studies with Tryptophan Analogs - Excited-State Interactions Involving the Side-Chain Amino Group, J. Phys. Chem., 99 (1995) 5713-5723.

[30] M.L. McLaughlin, M.D. Barkley, Time-resolved fluorescence of constrained tryptophan derivatives: Implications for protein fluorescence, Fluorescence Spectroscopy, 278 (1997) 190-202.

[31] J.R. Albani, Fluorescence Lifetimes of Tryptophan: Structural Origin and Relation with S-o -> L-1(b) and S-o -> L-1(a) Transitions, Journal of Fluorescence, 19 (2009) 1061-1071.

[32] J.N. Miller, J.C. Miller, Statistics and chemometrics for analytical chemistry, 5th ed., Pearson Prentice Hall, Harlow, England ; New York, 2005.

[33] R.A. Engh, L.X.Q. Chen, G.R. Fleming, Conformational Dynamics of Tryptophan - a Proposal for the Origin of the Nonexponential Fluorescence Decay, Chem. Phys. Lett., 126 (1986) 365-371.

[34] R.J. Robbins, G.R. Fleming, G.S. Beddard, G.W. Robinson, P.J. Thistlethwaite, G.J. Woolfe, Photophysics of Aqueous Tryptophan - pH and Temperature Effects, J. Am. Chem. Soc., 102 (1980) 6271-6279.

[35] D.M. Jameson, G. Weber, Resolution of the Ph-Dependent Heterogeneous Fluorescence Decay of Tryptophan by Phase and Modulation Measurements, J. Phys. Chem., 85 (1981) 953-958.

[36] H. Shizuka, M. Serizawa, T. Shimo, I. Saito, T. Matsuura, Fluorescence-Quenching Mechanism of Tryptophan - Remarkably Efficient Internal Proton-Induced Quenching and Charge-Transfer Quenching, J. Am. Chem. Soc., 110 (1988) 1930-1934.

[37] B. Valeur, G. Weber, Resolution of the fluorescence excitation spectrum of indole into the 1La and 1Lb excitation bands, Photochem. Photobiol., 25 (1977) 441-444.

[38] J.R. Alcala, E. Gratton, F.G. Prendergast, Fluorescence Lifetime Distributions in Proteins, Biophys. J., 51 (1987) 597-604.

[39] D.M. Togashi, A.G. Ryder, Time-resolved fluorescence studies on Bovine Serum Albumin denaturation process, Journal of Fluorescence, 16 (2006) 153-160.

[40] M.N. Berberan-Santos, B. Valeur, Luminescence decays with underlying distributions: General properties and analysis with mathematical functions, J. Lumin., 126 (2007) 263-272.

[41] A. de Juan, R. Tauler, Multivariate curve resolution (MCR) from 2000: Progress in concepts and applications, Crit. Rev. Anal. Chem., 36 (2006) 163-176.

[42] K.R. Murphy, C.A. Stedmon, D. Graeber, R. Bro, Fluorescence spectroscopy and multi-way techniques. PARAFAC, Analytical Methods, 5 (2013) 6557-6566.